P10.2 **GLOBAL PROPERTIES OF A SIMPLE AXISYMMETRIC SIMULATION OF TORNADOGENESIS**

Robert Davies-Jones*
National Severe Storms Laboratory, NOAA
Norman, Oklahoma

1. INTRODUCTION

This paper examines the evolution of global quantities in the simple numerical axisymmetric simulation of tornadogenesis presented by Davies-Jones (2000; hereafter DJ00). In this simulation, the domain is closed and the flow is homogeneous with constant density ρ and eddy viscosity ν. Rain with a specified radial and temporal distribution and constant fall velocity is introduced at the top. No-slip boundary conditions are applied to the zonal (tangential) motion and free-slip ones to the meridional (radial-vertical) motion. These boundary conditions permit the initial condition to be a Beltrami flow (Davies-Jones 2002) and the formation of an intense vortex. The equations are cast in the vorticity-streamfunction formulation. Lengths, velocities, times and pressure are nondimensionalized by the domain height H, the initial maximum vertical velocity W, the advective time scale H/W, and ρW^2. In the simulation the Froude number Fr $\equiv gH/W^2 = 100$, the Reynolds number Re $\equiv WH/\nu =$ 2000 and the Prandtl number Pr $\equiv \nu/\kappa = 1$ where g is the gravitational acceleration and κ is the diffusivity for liquid water. Crude scaling of the results to a supercell is done by setting $W = 34$ m s^{-1}, $H = 12$ km, and $\rho = 1$ kg m^{-3}. One unit of time is then 5.8 min, the rim is at 8.4 km, and the initial midlevel mesocyclone has a pressure deficit of 6 mb, an updraft radius of 5.3 km, and a maximum tangential velocity of 23 m s^{-1} at $r = 4.1$ km. The unstaggered grid consists of a square mesh of 201x285 points with $\Delta r = \Delta z = 42$ m when scaled to a supercell. Doubling or halving this resolution affects the results minimally. The model uses Arakawa's (1966) finite-difference Jacobian [with a new form (Davies-Jones 2001) for points on the axis] to prevent the false generation of global kinetic energy and angular momentum by the nonlinear advection terms, and outputs balanced global budgets of zonal, vertical and radial kinetic energy, helicity, enstrophy, angular momentum, water, and circulation around a vertical section.

---

*Corresponding author address: Dr. Robert Davies-Jones, NOAA/National Severe Storms Laboratory, National Weather Center, 120 David L. Boren Blvd., Norman, OK 73072-7323.
E-mail: Bob.Davies-Jones@noaa.gov

The initial condition is a Beltrami flow (BF). Its meridional circulation has an updraft maximum on the axis and a maximum compensating downdraft at the rim (see Fig. 1). The tangential flow is counterclockwise with maximum tangential velocity v near the edge of the updraft and cyclonic (anticyclonic) vorticity in the updraft (downdraft) region. Without rain, the flow remains a BF that undergoes a slow viscous decay with no change in pattern. By time $t = 6$ the velocity and pressure amplitudes decay by 11% and 21 %, respectively. Even though the downdraft transports angular momentum downward, there is no intensification of rotation at low elevations because there is no advection of angular momentum M (the streamlines and M-contours coincide in Fig. 1). Without rain, the twisting downdraft does not lead to vortex formation.

The initial balance of the BF is upset by introducing a realistic amount (maximum mixing ratio 5 g kg^{-1}) of density anomalies ("large raindrops") at the part of the top boundary above the updraft. At the top, the mixing ratio q has the same functional dependence on r as the initial

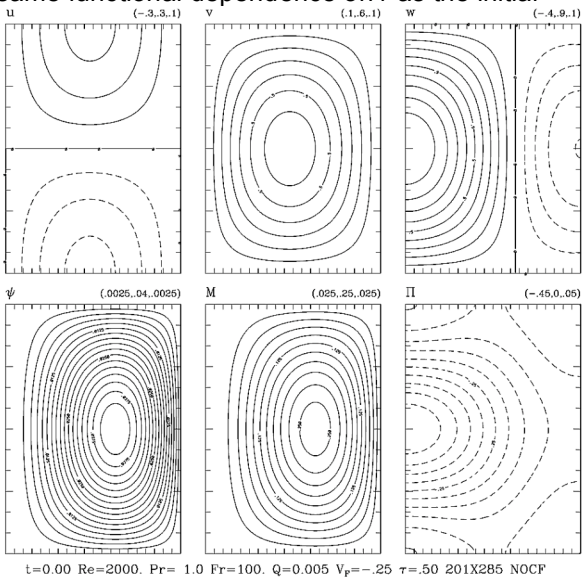

Fig. 1. Clockwise from top left: Initial fields of radial, tangential and vertical velocity (u, v, w), pressure Π, angular momentum M, and streamfunction ψ. The (minimum, maximum, contour interval) are (-.33, .33, .1), (0, .67, .1), (-.4, 1, .1), (-.5, 0, .05), (0, .26, .025) and (0., .042, .0025), resp. Negative contours are dashed. Tick marks are at intervals of 10 grid points along the ground and $H/12$ along the axis (from DJ00).

updraft. The anomalies fall with the constant terminal velocity of -0.25 *W* around the updraft in a concentric "rain curtain" about 5 km in radius (Fig. 2). The associated drag forces accelerate air with relatively high angular momentum (AM) toward the ground. Some of this high-angular-momentum air flows out of the curtain along the ground towards the axis where it is stretched vertically, and spins up into a tornado-like vortex (Fig. 3). The tornadogenesis culprit is undeniably the rain-induced downdraft. The vertical vorticity is anticyclonic in the rain-induced cyclonically revolving downdraft. The vorticity is tilted radially inward in the outflow and then upwards in the axial updraft.

From initial state to maximum tornado intensity, the maximum vertical velocity, the

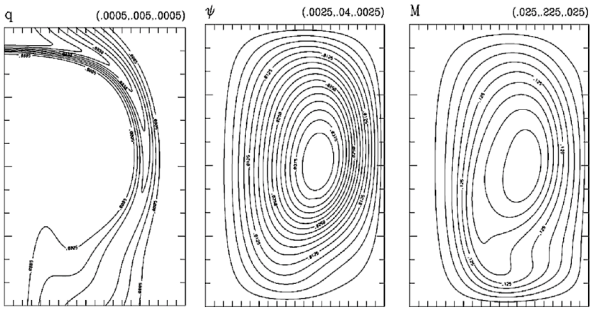

Fig. 2. Left to right: The q contours (from .0005 to .005 by .0005), ψ contours (from .0025 to .04 by .0025) and M contours (from .025 to .225 by .025) at $t = 4$.

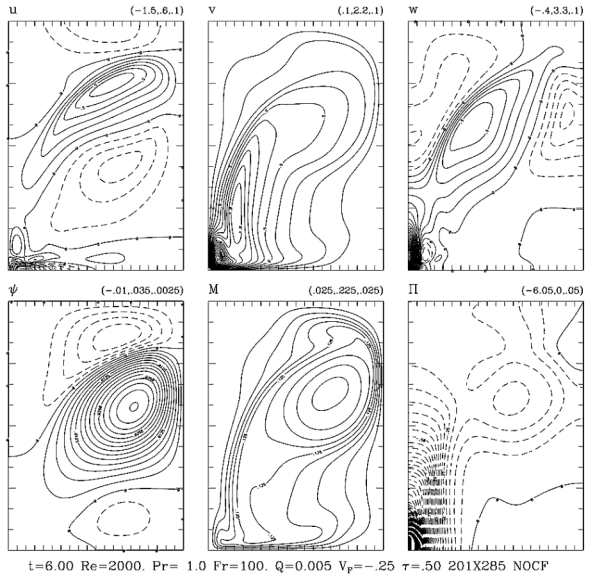

Fig. 3. As in Fig. 1, but at t = 6. The minimum, maximum contour values and the contour interval are (-1.5, .6, .1) for u, (.1, 2.2, .1) for v, (-.4, 3.3, .1) for w, (-6.05, 0, .05) for Π, (.025, .225. .025) for M and (-.01, .035, .0025) for ψ (from DJ00).

maximum tangential velocity, and the minimum pressure descend from mid level to near the ground and increase from 1 to 3.4, from .67 to 2.2, and from -.5 to -6, respectively. Initially, the maximum and minimum nonhydrostatic vertical pressure-gradient force (NHVPGF) per unit mass are ±1.6 at 3 and 9 km, respectively. At maximum tornado intensity, these values become 170 (or 1.7 *g*) in the axial jet and -100 (-*g*) just above the axial jet.

The vortex fills from above and decays as the pressure-driven axial downdraft penetrates to low levels. It dies owing to the lack of a buoyant cork (Fiedler 1995) as the downdraft reaches the surface and its divergent outflow dilutes the vertical vorticity. Absence of a buoyant cork does not prevent a strong vortex from forming, but the presence of one would prolong the vortex lifetime.

The model largely simulates Fujita's (1973, 1975) 'recycling hypothesis' of tornadogenesis (Fig. 4). Fujita observed that the overshooting top collapses prior to a major tornado and that the rotating rain curtain curves towards the tornado, suggesting a recycling inflow. In his conceptual model, the collapsing top triggers the tornado by intensifying the water-loaded cyclonically twisting downdraft. Air with high AM flows out of the downdraft near the ground. Some of it converges towards the axis, and enters the tornado, thus maintaining it. Fujita originally thought that the high-AM air at the surfaces originates from near storm top, but he later conceded that this was unrealistic from a thermodynamic viewpoint (Forbes and Bluestein 2001).

Vortex formation in the present computer model resembles that in a simulation (run MDL-2) by Das (1983). However, the Das simulation is dissimilar to the DJ00 one in many respects. Das used an open domain only 1.5 km tall with conditions at open boundaries imposed rather unrealistically. He thus uncoupled the tornado from its parent storm (Fiedler 1995). He also started from an initial mesocyclone devoid of the meridional motion necessary for its creation (vertical motion was initiated by unbalanced pressure-gradient forces in the initial state of 'height-dependent solid-body rotation'), introduced a precipitation gush at the top around the axis and relied on centrifuging of precipitation to create a rain curtain only 800 m in radius. The mechanism worked only for a very large maximum mixing ratio (16 g kg^{-1}) and associated rainfall rate (~500 mm h^{-1}). In the DJ00 model, centrifuging hardly affects the results and is turned off in the present simulation. Also, intense rainfall along the axis occurs only at the end after the total collapse of the central updraft and the death of the vortex.

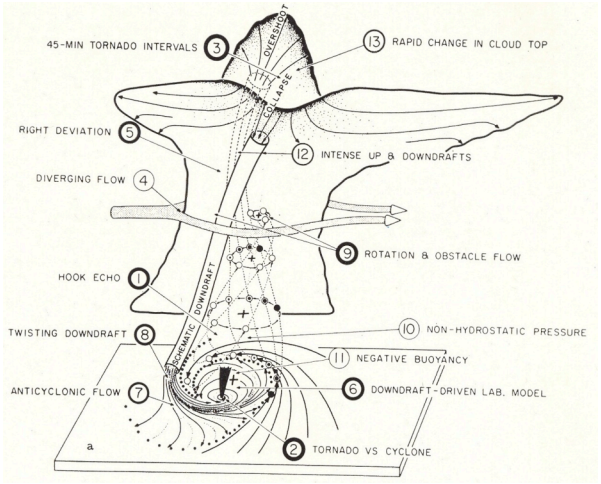

Fig. 4. Fujita's schematic of a tornadic thunderstorm (from Braham and Squires, 1974).

2. TIME-HEIGHT DIAGRAMS

Contours of the maximum mixing ratio as a function of time and height are shown in Fig. 5. The specified mixing ratio at the top approaches maximum amplitude (.005) in roughly 0.8 of a time unit. Strong surface rainfall (at rates ~ 60 mm h^{-1}) begins at around 4 time units because the fall speed in still air is 0.25 *W*. The maximum precipitation mixing ratio at low levels is less than 2 g kg^{-1} prior to and during tornadogenesis with the heavier concentrations of water staying aloft. Recycling of precipitation particles in the updraft is evident between *t* = 5 and 6. Intense rain commences after the tornado.

Fig. 6 presents contours of vertical velocity on the axis in time-height space. Between *t* = 4 and 5, the maximum axial velocity descends from mid to low altitudes without much intensification. The axial updraft weakens at high levels. This is the model equivalent of collapse of the overshooting top in supercells. The maximum updraft on axis then lowers further as an end-wall vortex and associated axial jet form. Beginning just prior to *t* = 4, the pressure deficit on the axis intensifies at mid levels and descends to near the ground as tornadogenesis proceeds (Fig. 7). The associated NHVPGF evolution is shown in Fig. 8. Above the end-wall vortex, downward axial pressure gradients force flow down the axis. This downdraft eventually reaches the surface and eliminates the vortex.

The air with the highest angular momentum (>.225) stays at mid levels throughout the simulation (Fig. 9). The precipitation-induced downdraft transports air with angular momentum of around .125 to near the surface between *t* = 3 and 6. Near-conservation of parcel angular momentum tells us that this air must descend at least 2 km.

The contours of maximum tangential velocity in time-height space (Fig. 10) provide indications of two vortices, namely a strengthening mesocyclone with maximum strength lowering from 6 to 3 km and a rapidly intensifying tornadic

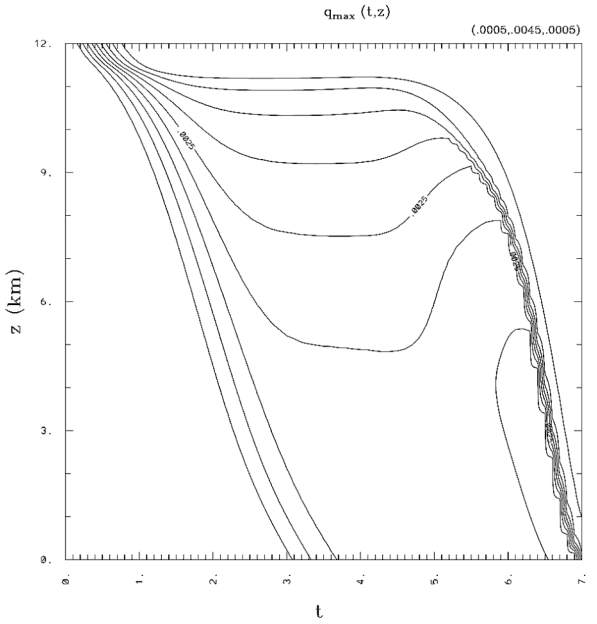

Fig. 5. Time-height diagram of maximum rain mixing ratio. For comparison with a supercell, the height of the domain has been scaled to 12 km and one time unit scales to 5.8 min. Contours are from .0005 to .0045 by .0005.

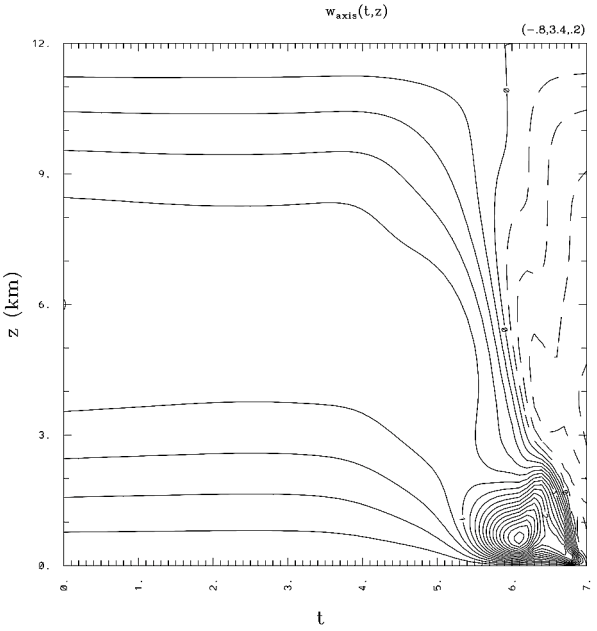

Fig. 6. Axial vertical velocity as a function of *t* and *z*. Contours are from -.8 to 3.4 by .2.

vortex at low levels. Examination of other figures (not shown) reveals that the mesocyclone is contracting as it intensifies. Its associated updraft narrows at low levels as it is squeezed by downdraft. In the atmosphere, this downdraft encroachment is visible as a clear slot and as cloud elements cascading down the side of the storm tower.

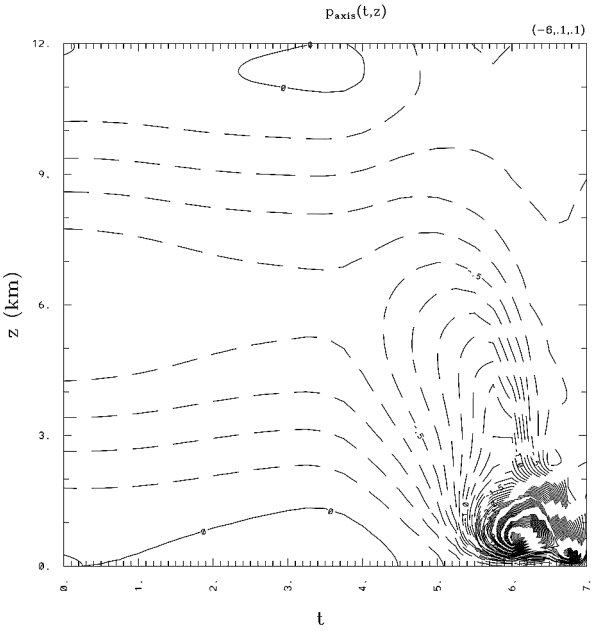

Fig. 7. Axial pressure as a function of *t* and *z*. Contours are from -6 to .1 by .1. Pressure is computed at time intervals of .25 (not at every time step).

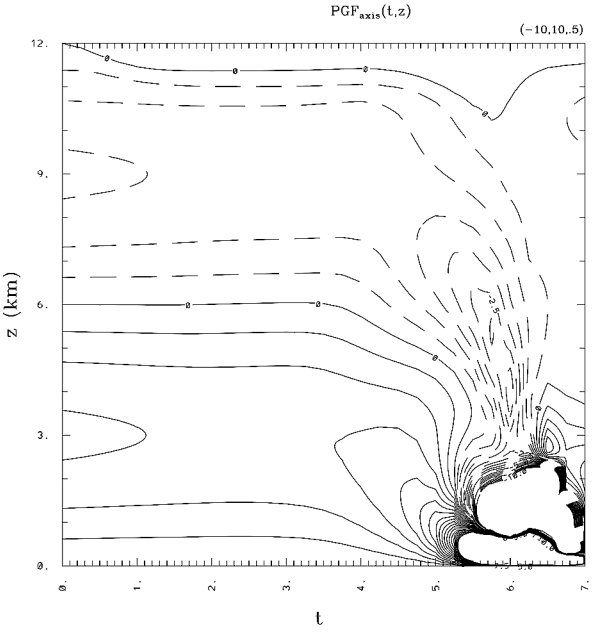

Fig. 8. Axial NHVPGF as a function of *t* and *z*. Contours are from -10 to 10 by .5. At the lower right side of the figure, values rise (fall) to 170 (-100) in the lower (upper) 'white hole'.

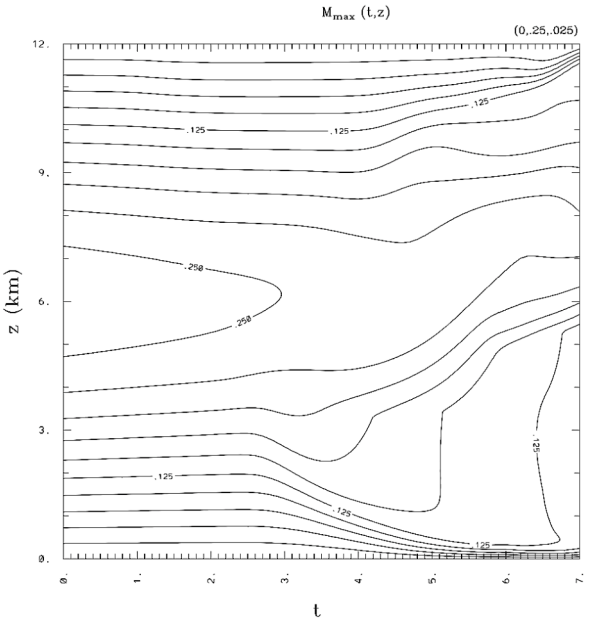

Fig. 9. Maximum angular momentum as a function of *t* and *z*. Contours are from 0 to .25 by.025.

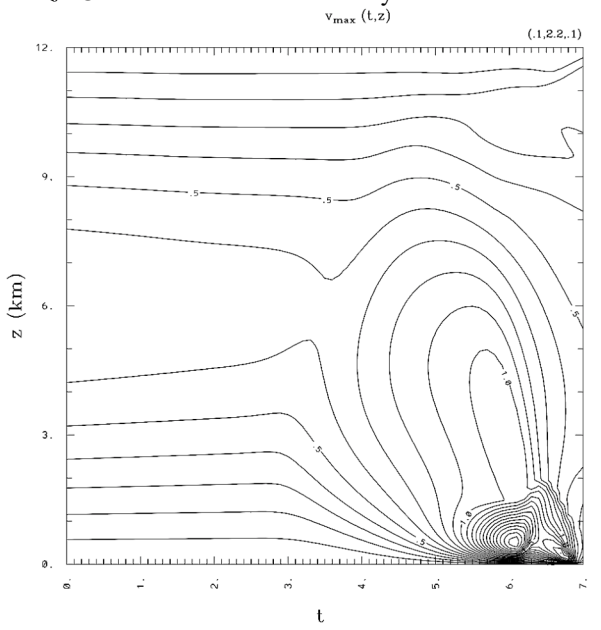

Fig. 10. Maximum tangential velocity as a function of *t* and *z*. Contours are from .1 to 2.2 by.1.

3. ENERGY AND OTHER BUDGETS

Global kinetic energy (GKE) is partitioned into the kinetic energy (KE) of the *u*, *v*, and *w* wind components (UKE, ZKE, WKE, respectively). An energy diagram is shown in Fig. 11. Frictional dissipation is a sink for all KE parts. The vertical KE (WKE) gains energy from the work done by the precipitation-drag force. This is the only

source of GKE. Also included in Fig.11 are the values at t = 6 for the no-rain case (BF), in which there are no energy transformations apart from frictional dissipation. The Beltrami flow has minimal gradients of velocity. Therefore, in the flow with rain there is significantly more dissipation. This increase in dissipation is less than the work input so the GKE is slightly larger in the simulation with rain than in the no-rain case.

Because the domain is closed, the pressure-gradient force does no net work, but converts WKE into radial KE (UKE) when rain is present. The centrifugal force acts at right angles to the motion and so never does any work, but does change UKE into zonal KE (ZKE). Figs. 11-14 show how the KE parts evolve from their initial values to their values at maximum vortex intensity (t = 6) and beyond. The vertical KE loses a lot more energy to UKE through the pressure term than it gains from work done by the drag force.

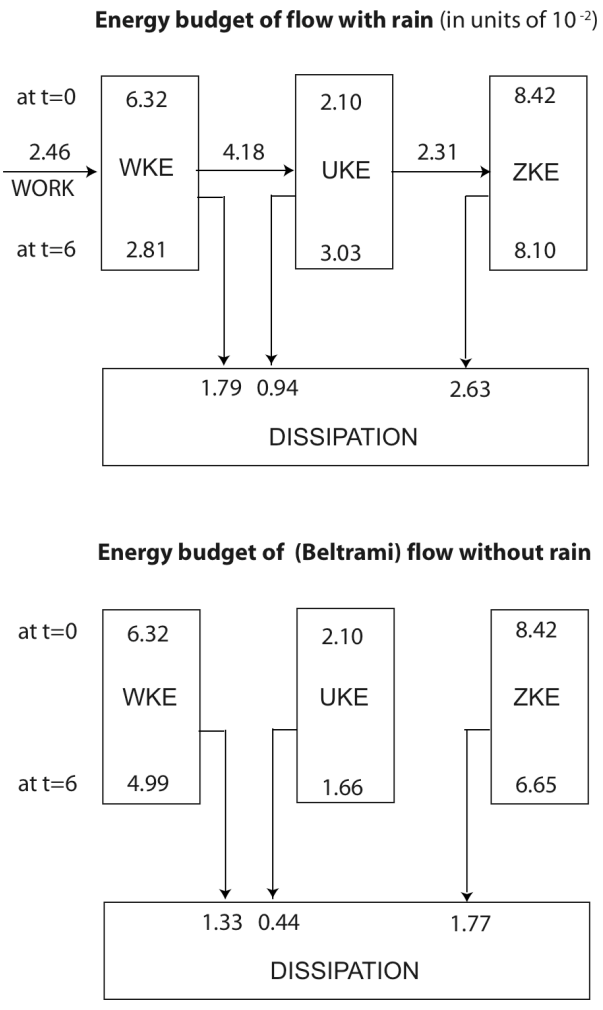

Fig. 11. Energy-budget diagrams for the simulation and for the equivalent simulation without rain.

Consequently, WKE is drastically reduced by the time the tornadic vortex is strongest, despite the extremely high WKE density in the axial jet. The overall WKE declines owing to the weakening of the storm-scale updraft, which affects WKE far

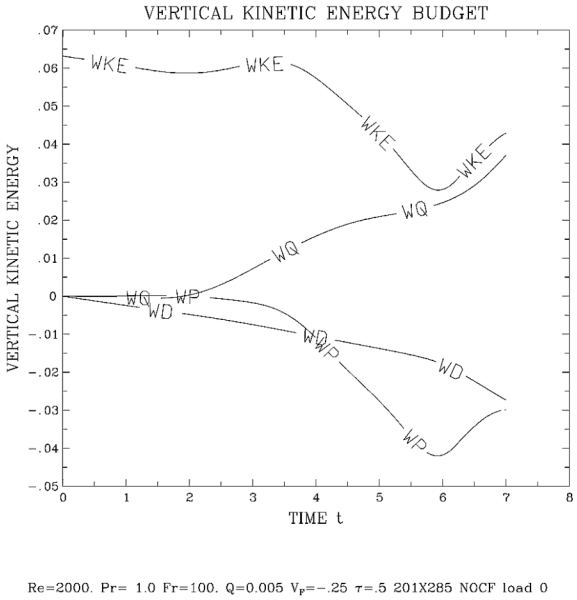

Fig. 12. Vertical KE budget as a function of time. WKE is the vertical KE, WQ is the accumulated gain in WKE owing to work done by the drag force, WP is the accumulated gain due to the pressure-gradient force (calculated as a residual), and |WD| is the accumulated loss due to frictional dissipation.

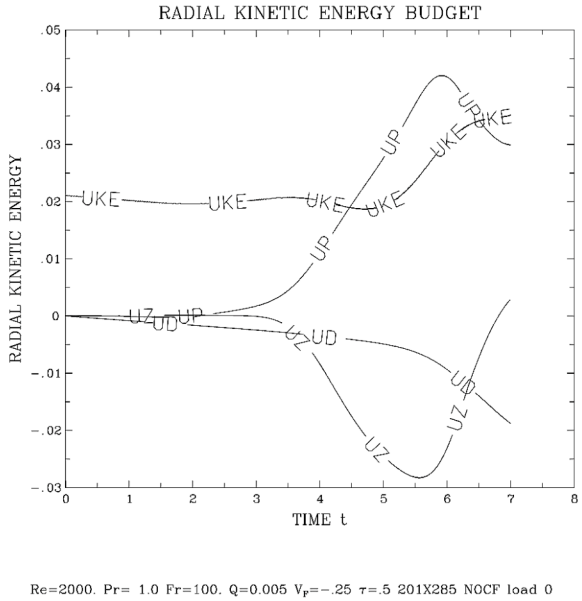

Fig. 13. Radial KE budget as a function of time. UKE is the radial KE, UZ is the gain in UKE owing to the centrifugal force, UP (= -WP) is the gain due to the pressure-gradient force, and |UD| is the loss due to frictional dissipation.

more than the axial jet does because the volume of the updraft is much larger. Tornado formation as the updraft declines has been observed often in Doppler-radar analyses. There is considerably more UKE at t = 6 than present initially owing to the gain from WKE more than compensating for losses to ZKE and dissipation. The zonal KE gains from UKE through the centrifugal term but loses more energy to dissipation so there is a slight loss of ZKE from t = 0 to t = 6. However, there is more ZKE in the simulation with rain than in the BF.

After t = 6, the vortex weakens and the WKE recovers somewhat as the central storm-scale updraft is replaced by intensifying axial downdraft at progressively lower levels. By t = 7, this downdraft has penetrated to the surface and eliminated the axial jet and vortex.

Helicity declines precipitously during tornado genesis and decay owing to losses associated with the diffusion term in the helicity equation. The term containing the drag force is positive but quite insignificant. At the same time, enstrophy increases dramatically because dynamical production associated with stretching of vortex filaments overcomes large diffusive losses. Mean angular momentum in the domain declines slowly owing to the frictional torque exerted at the boundaries.

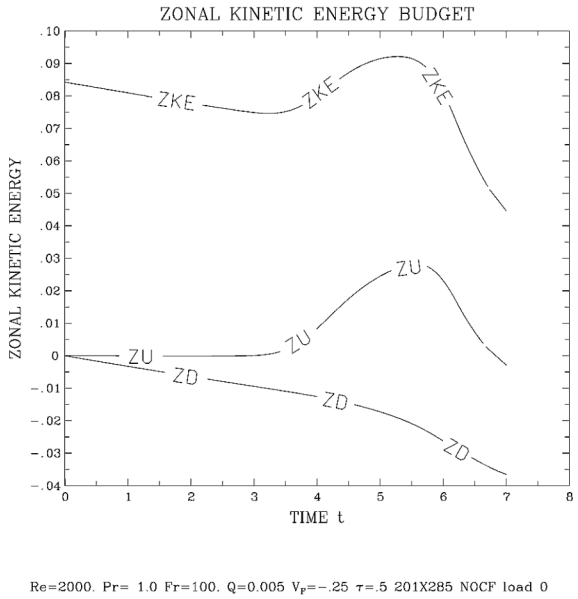

Fig. 14. Zonal KE budget as a function of time. ZKE is the zonal KE, ZU (= -UZ) is the gain in UKE owing to the centrifugal force, and |ZD| is the loss due to frictional dissipation.

4. SUMMARY

A simple axisymmetric model without buoyancy can simulate several observed features of tornadogenesis. Complex 3-D models of supercells naturally produce tornadoes more realistically, but without clear-cut physical explanation.

The most noteworthy global precursor of tornado formation is a dramatic decline in vertical kinetic energy despite a conversion of work by the drag force into WKE and the formation of a high-speed axial jet. This decline is accompanied by rapid intensification of the global maxima in vertical, inflow and tangential velocity and pressure deficit, as the 'recycling' process forms a concentrated low-level vortex with an axial jet. During this process, the updraft maximum and pressure minimum relocate along the axis from mid to low level, and the tangential-velocity maximum moves steadily inward and jumps down to near the ground.

Acknowledgments. This work was supported in part by NSF grant ATM-0340693.

5. REFERENCES

Arakawa, A., 1966: Computational design for long-term numerical integration of the equations of fluid motion: Two-dimensional incompressible flow. Part I. *J. Comput. Phys.*, **1**, 119-143.

Braham, R. R., Jr., & P. Squires, 1974: Cloud physics -- 1974. *Bull. Amer. Meteor. Soc.*, **55**, 543-586

Das, P., 1983: Vorticity concentration in the subcloud layer of a rotating cloud. Final report of NSF Grant No. ATM-8023825, National Science Foundation, Washington, D.C. 20550, 78 pp.

Davies-Jones, R. P., 2000: Can the hook echo instigate tornadogenesis barotropically? *Preprints,* 20th Conf. Severe Local Storms, Orlando, FL, Amer. Meteor. Soc., 269-272.

Davies-Jones, R., 2001: Computation of a solenoid as a ratio of areas and a geometric interpretation of the Arakawa Jacobian. *Mon. Wea. Rev.,* **129,** 345-353.

Davies-Jones, R., 2002: Linear and nonlinear propagation of supercell storms. *J. Atmos. Sci.,* **59**, 3178-3205.

Fiedler, B. H., 1995: On modeling tornadoes in isolation from their parent storm. *Atmosphere-Ocean,* **33**, 501-512.

Forbes, G. S., and H. B. Bluestein, 2001: Tornadoes, tornadic thunderstorms, and photogrammetry: A review of the contributions of T. T. Fujita. *Bull. Amer. Meteor. Soc.*, **82**, 73-96.

Fujita, T. T., 1973; Proposed mechanism of tornado formation from rotating thunderstorm. *Preprints*, 8th Conf. on Severe Local Storms, Denver, CO, Amer. Meteor. Soc., 191-196.

Fujita, T. T., 1975; New evidence from April 3-4, 1974 tornadoes. *Preprints*, 9th Conf. on Severe Local Storms, Norman, OK, Amer. Meteor. Soc., 248-255.